Aust. J. Phys., 1996, **49**, 51–77

Chaos and Its Impact on the Foundations of Statistical Mechanics*

Gary P. Morriss and Lamberto Rondoni

School of Physics, University of New South Wales,
Sydney, NSW 2052, Australia.

Abstract

In this work we present a brief derivation of the periodic orbit expansion for simple dynamical systems, and then we apply it to the study of a classical statistical mechanical model, the Lorentz gas, both at equilibrium and in a nonequilibrium steady state. The results are compared with those obtained through standard molecular dynamics simulations, and they are found to be in good agreement. The form of the average using the periodic orbit expansion suggests the definition of a new dynamical partition function, which we test numerically. An analytic formula is obtained for the Lyapunov numbers of periodic orbits for the nonequilibrium Lorentz gas. Using this formula and other numerical techniques we study the nonequilibrium Lorentz gas as a dynamical system and obtain an estimate of the upper bound on the external field for which the system remains ergodic.

1. Introduction

Our aim in this paper is to study the properties of chaotic dynamical systems, with particular emphasis upon mechanical systems that evolve continuously in time. However, it is often true that the easiest demonstration of the necessary techniques is that for simple mappings. Therefore, although there are subtle differences between the behaviour of mappings and flows, we introduce the theoretical tools which we use by applying them to the quadratic map. In particular, we concentrate on the recently developed **periodic orbit expansion** (POE) theory (Hannay and Ozorio de Almeida 1984; Artuso *et al.* 1990; Cvitanovic 1992; Cvitanovic *et al.* 1992). Then, one can always think of a mapping as an approximation to a continuous time system, as if it constituted a numerical scheme to solve continuous time evolution equations. For instance $x_{n+1} = x_n + \mu F(x_n)$ can be interpreted as the Euler (one-step finite difference) scheme for the numerical solution of $\mathrm{d}x/\mathrm{d}t = kF(x)$, where $\mu = k\Delta t$. Alternatively, F could implicitly be defined in terms of the equations of motion of a given physical system, and give the *exact* variation of x in a given interval of time. Then, the mapping would not be just an approximation to a given time evolution, but it would yield the exact values of x for a discrete set of times. It is within such a framework that we also make use of mappings to represent continuous time evolutions of physical models.

* Refereed paper based on a contribution to the fourth Gordon Godfrey Workshop on Atomic and Electron Fluids, held at the University of New South Wales, Sydney, in September 1994.

0004-9506/96/010051$10.00

The idea of studying statistical mechanical models using the theory of chaos is justified in part by recent results, such as the discovery of the conjugate pairing rule for the Lyapunov exponents of nonequilibrium systems (Evans *et al.* 1990), and an equivalent result obtained by Gaspard (Gaspard and Rice 1989). These connections between transport coefficients and nonlinear stability properties have provided new reasons for studying model systems such as the Lorentz gas (Lorentz 1905; Machta and Zwanzig 1983). Several different approaches have been used, in particular the POE method (Vance 1992; Morriss and Rondoni 1994; Rondoni *et al.* 1995) based on the idea of singular measures, which we illustrate for the quadratic map in Section 2. In Section 3 we introduce the Lorentz gas both at and away from equilibrium, and we present some numerical results for the system, obtained using standard molecular dynamics techniques. Section 4 is devoted to the nonequilibrium Lorentz gas, where molecular dynamics is used to calculate the diffusion coefficient, the pressure, and the conductivity as a function of an applied external field. In Section 5 we discuss the application of the POE method to the equilibrium Lorentz gas, and we show how it can be used to calculate thermodynamic averages. This is followed, in Section 6, by the development of a new dynamically (periodic orbit) based partition function, and numerical tests of this function are reviewed. In Section 7 we show that analytic expressions can be obtained for the Lyapunov numbers of periodic orbits of the nonequilibrium Lorentz gas, which give a very powerful tool in the application of the POE, and in the understanding of the Lorentz gas model as a two-dimensional mapping. Section 8 reports our POE results for the nonequilibrium case, Section 9 deals with the Lorentz gas as a two-dimensional dynamical system, and Section 10 concludes the paper.

2. The Quadratic Map

Consider a one-dimensional mapping $x_{n+1} = f(x_n)$, such as the quadratic map, where f takes the form $f(x) = \mu x(1-x)$ and $x \in [0,1]$. Imagine that we have a normalised initial distribution where only one point, x_0, has a nonzero probability. This distribution function can be written as a delta function at x_0, that is $\delta(x - x_0)$. Under the action of the mapping this distribution will change and after one application the delta function will have moved to the new point $f(x_0)$. The operation of the mapping on the delta function distribution can be written as

$$\delta(x - f(x_0)) = \int_0^1 \mathrm{d}s\, \delta(x - f(s))\, \delta(s - x_0)\,. \tag{1}$$

Clearly, in this equation, the second delta function selects that value of s that is equal to x_0 and substitutes this value for s in the first delta function. The delta function shifts from the position of the initial point x_0, to the position that x_0 is mapped to by one application of the mapping, that is $f(x_0)$. In a similar way we can ask what is the distribution after n applications of the mapping, and the result is a delta function at $f^n(x_0)$ so that

$$\delta(x - f^n(x_0)) = \int_0^1 \mathrm{d}s\, \delta(x - f^n(s))\, \delta(s - x_0)\,. \tag{2}$$

We can immediately generalise this procedure by imagining the operation of the mapping upon some initial distribution function $\rho_0(x)$ (perhaps composed of a weighted sum of delta functions). Clearly the initial distribution will be transformed to a new distribution $\rho_1(x)$ after one iteration of the map, where

$$\rho_1(x) = \int_0^1 \mathrm{d}s\, \delta(x - f(s))\, \rho_0(s)\,. \tag{3}$$

After n iterations the initial distribution will be transformed to $\rho_n(x)$, where

$$\rho_n(x) = \int_0^1 \mathrm{d}s\, \delta(x - f^n(s))\, \rho_0(s)\,. \tag{4}$$

In this example the distribution continually changes with time, but in statistical mechanics we are interested in steady or stationary behaviour, and therefore it is important to find stationary solutions for the distribution function. That is, we require the solutions (if they exist) of

$$\rho(x) = \int_0^1 \mathrm{d}s\, \delta(x - f(s))\, \rho(s)\,. \tag{5}$$

In practice there will be a number of solutions of equation (5), as for example $\rho(x) = \delta(x - x^*)$, where x^* is a fixed point $[f(x^*) = x^*]$, is a solution. If there is more than one fixed point, then any linear combination of delta functions, based on those points, will also be a solution. Similarly, solutions based upon nth order periodic points $[f^n(x_i^*) = x_i^*]$ can also be constructed. These are a particular class of *singular* measures. In general, however, there will be a *natural* distribution (or measure) to which most points in the interval [0, 1] will converge. This *natural* measure does not emerge easily from equation (5), whereas solutions based upon periodic points are relatively easy to find. Our goal will be to generate a sequence of *singular* measures based upon periodic points, which approach the *natural* measure. By that, we mean that the sequence of averages, calculated using the sequence of singular measures, approaches the average calculated from the *natural* measure, for any system property.

To start, consider a singular measure of the form

$$\rho^{(n)}(x) = \sum_j C_j \sum_{i=1}^{n} \delta(x - s_{ij})\,, \tag{6}$$

where $\{s_{j1}, ..., s_{jn}\}$ are the n points of the jth n-cycle, and C_j is its normalised weight. This nth order singular distribution is the generic nth term in an infinite sequence of approximate distributions. Is $\rho^{(n)}(x)$ a solution of equation (5)?

$$\rho(x) = \int_0^1 \mathrm{d}s\, \delta(x - f(s)) \sum_j C_j \sum_{i=1}^{n} \delta(s - s_{ij})$$

$$= \sum_j C_j \sum_{i=1}^{n} \int_0^1 \mathrm{d}s\, \delta(x - f(s))\, \delta(s - s_{ij})$$

$$= \sum_j C_j \sum_{i=1}^{n} \delta(x - f(s_{ij}))$$

$$= \sum_j C_j \sum_{i=1}^{n} \delta(x - s_{ij}) = \rho^{(n)}(x)\,.$$

The third equality comes from using the delta function $\delta(s - s_{ij})$ in the integral, and the last equality follows because f simply permutes all the points in a cycle. Hence the singular measure is a solution, but we still need information about the weights C_j.

To introduce the concept of a measure consider a system of N particles divided into two boxes labelled 1 and 2. If ρ_1 is the measure of box 1, and ρ_2 is the measure of box 2, then the number of particles in box 1 is $N_1 = \rho_1 N$ and the number of particles in box 2 is $N_2 = \rho_2 N$. If we evolve the system in time, then after some initial transient, some particles from box 1 remain in box 1 and others move to box 2. The number remaining in box 1 is $N_{1\to 1} = \mu_1 N_1$, while $N_{1\to 2} = \mu_2 N_1$ transfer from box 1 to box 2. Regardless of the initial distribution N_i, the definition of the natural measure μ_i is given by the limit as $t \to \infty$, of $N_{i\to i} \equiv \mu_i N_i$. If the natural measure is unknown, we may determine it by

$$\mu_i \equiv \lim_{t\to\infty} \frac{N_{i\to i}}{N_i}\,. \tag{7}$$

The same process can be used to find the C_j. We construct a set of boxes on each of the periodic points of order n and find the number of points which return to the box after n applications of the map. Consider a single periodic point s_i, and an interval Δx which contains only that periodic point of length n. The number of points in that interval is

$$N_i = N \int_{\Delta x} \rho(x)\, \mathrm{d}x$$

where N is the total number of points in $[0,1]$. From equation (4), after n iterations of the map, the measure is

$$\rho(x)\,\Delta x = \int_{\Delta s'} \mathrm{d}s\; \delta(x - f^n(s))\, \rho(s)\, \Delta x\,,$$

where ρ is used in both sides of the equation because it is stationary. Here $\Delta s'$ is the intersection of $\Delta x'$ with the range of values of s that map into the interval Δx. That is, the points $\Delta s'$ are the only points of Δx which come back after n iterations. Using the identity

$$\delta(G(s)) = \sum_i \frac{\delta(s - s_i)}{|G'(s_i)|} = \sum_i \frac{\delta(s - s_i)}{\Lambda_i}\,, \tag{8}$$

where s_i is a zero of $G(s)$, but is not a zero of $|G'(s)| = \Lambda$, and considering that $\Delta s'$ contains the periodic point s_i, but no other preimages of x under f^n, we have

$$\rho(x)\,\Delta x = \int_{\Delta s'} \mathrm{d}s\, \frac{\delta(s-s_i)}{\Lambda_i}\,\rho(s)\,\Delta x = \frac{\rho(s_i)\,\Delta x}{\Lambda_i}\,.$$

Therefore the number of points remaining in Δx after n iterations of the map is

$$N_{i\to i} = N\int_{\Delta x}\rho(x)\,\mathrm{d}x = N\int_{\Delta x}\frac{\rho(s_i)dx}{\Lambda_i} = N\,\frac{\rho(s_i)\Delta x}{\Lambda_i} \approx \frac{N_i}{\Lambda_i}\,.$$

Here the $\approx$ becomes $=$ in the $n\to\infty$, $\Delta x\to 0$ limit. Repeating the process for all the points in the cycle we find that the weight associated with the jth periodic cycle is

$$C_j = \frac{N_{j\to j}}{N_j} = \frac{1}{\Lambda_j}\,,$$

where

$$\Lambda_j = |f^{n'}(s_{ji})| = \prod_{i=1}^{n}|f'(s_{ji})| \tag{9}$$

is the Lyapunov number for the cycle j which is independent of the point i. The singular measure that we need is then

$$\rho^{(n)}(x) = C\sum_j \Lambda_j^{-1}\sum_{i=1}^{n}\delta(x-s_{ij})\,, \tag{10}$$

where C is the normalisation. In this way we generate a sequence of stationary singular measures by considering all values of n. Note that at every n we exclude the periodic points of period m where m divides n. The periodic points of period m have already been used in the mth approximate (they are not *prime* orbits of length n), so we do not consider them again in the nth approximate.

Table 1. Structure of periodic cycles for the quadratic map at $\mu = 4$

Order	Solutions	Number of cycles									
		1	2	3	4	5	6	7	8	9	10
1	2	2									
2	4	2	1								
3	8	2		2							
4	16	2	1		3						
5	32	2				6					
6	64	2	1	2			9				
7	128	2						18			
8	256	2	1		3				30		
9	512	2		2						56	
10	1024	2	1			6					99

To develop the sequence of singular measures for the quadratic map we need to know a few details concerning periodic points. The mapping is quadratic, so in general there are two fixed points. If we find the fixed points of two applications of the map, then these fixed points are the periodic points (of period or length 2) of the map. The equation we need to solve is a quadratic with each x replaced

by the original quadratic, and is hence of order four with four solutions. Two of these solutions will be the original fixed points, the new points are a 2-cycle. At each order n there are 2^n solutions of $f^n(x) = x$ which imply a set number of cycles of various lengths. For the quadratic mapping at $\mu = 4$ all the solutions are real and the structure of cycles is given in Table 1.

If we calculate the average value of some quantity w using the singular measure from equation (10), the result is

$$\langle w \rangle = \int_0^1 \mathrm{d}x\, \rho(x)\, w(x) = C \sum_{j \in P_n} \Lambda_j^{-1} \sum_{i=1}^{n} w(s_{ij})\,, \tag{11}$$

where P_n is the set of all prime distinct cycles of length n. The normalisation constant is easily found by considering the case where $w = 1$. The final result for the nth order average of w is

$$\langle w \rangle_n = \sum_{j \in P_n} \Lambda_j^{-1} \sum_{i=1}^{n} w(s_{ji}) \Big/ \sum_{j \in P_n} \Lambda_j^{-1} n = \sum_{j \in P_n} \Lambda_j^{-1} n \langle w \rangle_j \Big/ \sum_{j \in P_n} \Lambda_j^{-1} n\,. \tag{12}$$

From equation (12) we can identify the true probability of a particular periodic cycle as

$$\rho_j = n\Lambda_j^{-1} \Big/ \sum_{j \in P_n} n\Lambda_j^{-1}\,. \tag{13}$$

Table 2. Periodic orbit expansion applied to the quadratic map at $\mu = 4{\cdot}0$

n	$\langle x \rangle$	$\langle x^2 \rangle$	# cycles
2	0·62500	0·46875	2
3	0·54167	0·40625	6
4	0·50000	0·37500	12
5	0·50833	0·38125	30
6	0·50354	0·37766	52(54)
7	0·51240	0·38430	120(126)
8	0·51017	0·38263	230(240)
9	0·50914	0·38185	482(504)
10	0·50904	0·38178	940(990)
11	0·50795	0·38097	1962(2046)
12	0·50731	0·38049	3853(4020)
exact	0·5	0·375	

For the quadratic map at $\mu = 4{\cdot}0$ we can calculate the average value of x and the average of its square exactly using the known analytic distribution function, and also numerically using the periodic orbit expansion. This exercise well illustrates the use of the singular measure to calculate average values. The results are given in Table 2. Here we have used periodic points of order 2 to 12, and we can study the convergence of this procedure. Notice also, that the number of cycles found numerically differs from the exact number (given in parenthesis) for order 6 and larger. This is a common numerical difficulty, which can easily be remedied for the quadratic map, but in general symbolic dynamics is used to help enumerate all the periodic points. For more complicated systems,

the symbolic dynamics is often not completely understood and determining all the physically allowed cycles has not been done in a systematic way.

We have introduced the idea of the periodic orbit expansion for the quadratic map. This is one example of an approach to the construction of the natural measure for many hyperbolic chaotic systems using approximations based upon measures supported on the unstable periodic orbits (UPOs). The reason why the method is expected to work is that the relevant attractor can be hierarchically approximated through sets of progressively longer and longer UPOs (Grebogi *et al.* 1988; Morriss *et al.* 1995), and the (weak) limit of these measures can be proved to be the natural measure for Axiom-A flows (Parry 1986). As we have seen the UPOs are grouped into sets of prime orbits P_n, and one attaches a stability weight to each UPO which is inversely proportional to the product of its expanding Lyapunov numbers Λ_i. The process of generating the average formula for a continuous time system is the same, and effectively results in replacing n by the period r and replacing sums by integrals, that is

$$\sum_{i=1}^{n} w(s_{ji}) \quad \text{by} \quad \int_0^{\tau_j} \mathrm{d}t\, w(t)\,.$$

What needs to be done then is to consider the set of UPOs of finite n, and then to extrapolate the results to the $n \to \infty$ limit. If B is a function of phase only, then the average value of B over the chaotic set can be written as

$$\langle B \rangle = \lim_{n\to\infty} \sum_{i\in P_n} \Lambda_i^{-1} \int_0^{\tau_i} B(s)\, \mathrm{d}s \Big/ \sum_{i\in P_n} \tau_i\, \Lambda_i^{-1}\,, \tag{14}$$

where τ_i is the period for the ith UPO, over which the integral is performed.

3. The Lorentz Gas

The Lorentz gas can be considered as a classical model for electrons moving independently through a crystal, and can be extended to simulate the motion under an applied electric field. In nonequilibrium statistical mechanics, self diffusion in fluids can be studied as the limiting case of mutual diffusion where the two species only differ in a *colour* label (Evans and Morriss 1990), and the smallest non-trivial system of this type contains two particles (one of each colour) (Moran and Hoover 1987). This two particle system in periodic boundary conditions is exactly equivalent to the Lorentz gas when the *colour field* is zero, and its extension to nonzero fields leads to a more complicated dynamics for the wandering particle between collisions. The Lorentz gas is clearly one of the simplest deterministic systems which exhibits diffusion in the absence of a field and a steady current away from equilibrium, and has therefore been recently re-examined to study irreversibility.

The equations of motion for the Lorentz gas give straight line trajectories between collisions, and the usual elastic collision rule. The constraint of either constant energy (or constant kinetic energy) for a two particle system implies that the speed of the wandering particle is constant. For cubic periodic boundary conditions the wandering point particle always has an infinite *horizon* (that is, for special initial conditions it can pass through the whole lattice without a

collision). To avoid this we adopt a triangular lattice, and choose the density sufficiently large so that the *horizon* is finite. We refer to the elementary cell (EC) as the hexagon whose replicas tile the whole two-dimensional plane. As the speed of the wandering particle is constant, the momentum has only one degree of freedom: its direction. So we can write $\boldsymbol{p} \equiv (p_x, p_y) = p(\cos\theta, \sin\theta)$ where θ is the angle between the x axis and the momentum vector (see Fig. 1). In turn, the position of the moving particle is more conveniently represented in polar coordinates, so $(x, y) = r(\cos\phi, \sin\phi)$. Thus, r, ϕ and θ are the only degrees of freedom of the model. The thermodynamic state point for the Lorentz gas can be characterised in terms of the disk spacing w, so if d is the distance between the centres, then $w = d - 2\sigma$. In what follows we take the radius $\sigma = 1$, and it is straightforward to show that the density is related to the spacing by $\rho = [2/(w+2)]^2/\sqrt{3}$. For large scatterer spacing (or low density), the Lorentz gas has an infinite horizon. To get a finite horizon we need $w \leq 4/\sqrt{3} - 2$.

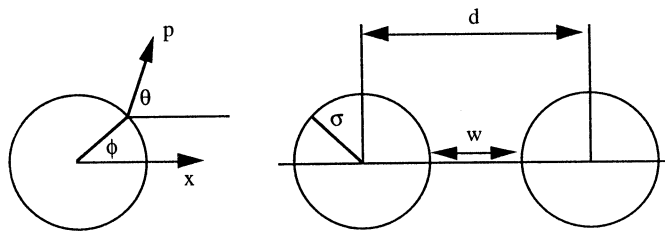

Fig. 1. Geometry of the Lorentz gas. For the scatterer at collision, the polar angle ϕ gives the position, while θ gives the angle between the momentum vector and the x axis. The system is parametrised by w/σ, where w is the spacing between scatterers.

In the presence of a field the wandering particle is acted upon by the combined effects of the external field and the thermostat. The thermostat ensures stationarity, by requiring that the kinetic energy of the particle is a constant of motion (so that the speed is fixed). The equations of motion for the Lorentz gas subject to an applied external field f_e pointing in the negative x-direction, with an isokinetic (Gaussian) thermostat, are given by

$$\dot{x} = p_x/M, \qquad \dot{p}_x = F_x - f_e - \alpha p_x\,,$$
$$\dot{y} = p_y/M, \qquad \dot{p}_y = F_y - \alpha p_y\,, \tag{15}$$

where (F_x, F_y) is the impulse force due to a collision with a scatterer, and the constraint of constant kinetic energy is imposed by choosing

$$\alpha = \frac{\boldsymbol{p}\,.\,\boldsymbol{F} - f_e\, p_x}{p^2}\,.$$

We take the fixed magnitude of the momentum p of the wandering particle, and its mass M, to be unity. Then, the temperature is given by $kT = 1$. Changing to polar coordinates for the momentum gives

$$\dot{\theta} = \epsilon \sin\theta\,, \tag{16}$$

where $\epsilon = f_e/p$. This equation can be integrated over a given interval of time, $\Delta t = t_1 - t_0$, and it yields

$$\tan(\theta_1/2) = \tan(\theta_0/2)\mathrm{e}^{\epsilon\Delta t}\,. \tag{17}$$

Integrating the equations of motion for the cartesian coordinates (in the absence of a collision), we find that the changes in x and y are parametrised by the angle θ, so

$$x_1 - x_0 = \frac{p}{M\varepsilon}\ln\left(\frac{\sin\theta_1}{\sin\theta_0}\right) \quad \text{and} \quad y_1 - y_0 = \frac{p(\theta_1 - \theta_0)}{M\varepsilon}\,. \tag{18}$$

Here we summarise the best available results of numerical simulations for the Lorentz gas. There are a variety of direct simulation methods that can be used to compute the diffusion coefficient D at equilibrium. In particular, the value of D obtained from a combination of the use of the Einstein relation and the Green–Kubo formula. The Einstein relation for D in two dimensions can be written as

$$D = \lim_{t\to\infty} \tfrac{1}{4}\frac{\langle \Delta \boldsymbol{r}(t)^2\rangle}{t}\,, \tag{19}$$

where $\langle\ \rangle$ indicates an ensemble average, and $\Delta\boldsymbol{r}(t)$ is the displacement of the wandering particle in time t. The Green–Kubo formula for the same quantity is

$$D = \int_0^\infty \mathrm{d}s\ \tfrac{1}{2}\langle \boldsymbol{v}(0)\,.\,\boldsymbol{v}(s)\rangle\,, \tag{20}$$

where $\boldsymbol{v}(s)$ is the velocity of the wandering particle at time s. Any ensemble which is modelled in a computer simulation necessarily contains a finite number of elements, thus an ensemble average actually means an approximation of phase space integral by a finite sum. Similarly, we cannot take the limit as $t \to \infty$ in the Einstein relation, but only estimate it based on the ratio at large time. Here we construct an ensemble of systems uniformly distributed in that part of phase space not occupied by the scatterer, and uniformly distributed over the surface of the unit ball in momentum space. It is found that the mean square displacement converges quickly with increasing ensemble size, but slowly with increasing T, while the Green–Kubo integral converges quickly with increasing T, but slowly with increasing ensemble size. Thus to get the best estimate of D we choose a sufficiently large value of the quickly convergent variable, and then extrapolate the diffusion coefficient as a function of the inverse of the slow variable. The Green–Kubo diffusion coefficient converges like a random variable with increasing ensemble size, while the mean square displacement is a monotonically increasing linear function of T. In this paper we will concentrate on a system where $w = 0{\cdot}2360685$, where the best result for D is $0{\cdot}197\pm0{\cdot}001$.

The instantaneous expression for the pressure tensor $\boldsymbol{P}(t)$ can be written as a function of the instantaneous values of position and momentum to obtain

$$\boldsymbol{P}V = \sum_{i=1}^{N}\frac{\boldsymbol{p}_i\,\boldsymbol{p}_i}{m} - \tfrac{1}{2}\sum_{i,j=1}^{N}\boldsymbol{r}_{ij}\,\boldsymbol{F}_{ij}\,, \tag{21}$$

where V is the volume of the system, $\boldsymbol{F}_{ij}$ is zero except at a collision, and $\boldsymbol{p}_i$ is constant between two collisions.

4. The Nonequilibrium Lorentz Gas

In an external field, we obtain the conductivity $L(\varepsilon)$ as the ratio of the mass current to the external field $L(\varepsilon) = J(\varepsilon)/\epsilon$, where the mass current,

$$\boldsymbol{J}(\varepsilon) = \lim_{t \to \infty} \Delta \boldsymbol{r}(t)/t\,.$$

The usual diffusion coefficient D is given by the zero field limit of $L(\varepsilon)$. Further, the field dependent conductivity $L(\varepsilon)$ depends upon the direction of the external field, with respect to the lattice of scatterers. We need only consider the angle α between one of the lines joining the centres of two nearest neighbour scatterers and the field direction, in the range $0 \leq \alpha \leq \pi/6$, as any other angle can be mapped into this range using the lattice symmetries. At the ends of this range, $\alpha = 0$ and $\alpha = \pi/6$, the triangular lattice of scatterers is symmetric with respect to reflection in the field direction. At any other value of α however, this symmetry is broken and the conductivity $L(\varepsilon)$ becomes a second rank tensor, so that

$$\begin{pmatrix} J_x \\ J_y \end{pmatrix} = \begin{pmatrix} L_{xx} & L_{xy} \\ L_{yx} & L_{yy} \end{pmatrix} \begin{pmatrix} \varepsilon_x \\ \varepsilon_y \end{pmatrix} \tag{22}$$

In all our calculations the field direction is taken to be along the x-axis and we calculate the two mass currents J_x and J_y, which allows us to calculate L_{xx} and L_{yx}. Although when $\varepsilon = 0$ we have $L_{xx} = L_{yy} = D$ and $L_{xy} = L_{yx} = 0$, at other values of the field these equalities do not hold. In the literature only the values $\alpha = 0$ (Baranyai *et al.* 1993; Cvitanovic *et al.* 1992; Morriss and Rondoni 1994) and $\alpha = \pi/6$ (Moran and Hoover 1987; Vance 1992) have been considered.

The results in Figs 2 and 3 give the diffusion coefficient as a function of field at $\alpha = 0$ and $\alpha = \pi/6$. In both cases there is a great deal of structure in conductivity versus field curves. The source of the structure is the result of a competition between the detailed variation in the probability of particular trajectories, and the shape of the channels between the scatterers that these trajectories must move in. Some understanding of these mechanisms can be obtained by considering small periodic orbits, as a function of field. In Figs 4 and 5 we present the conductivities L_{xx} and L_{yx} as a function of angle at a fixed field of $\varepsilon = 1$. We see the appearance of a local maximum at approximately $\alpha = 0{\cdot}2$ and a local minimum at approximately $\alpha = 0{\cdot}44$. The existence and position of the relative maximum and minimum remain at other values of the field but no exhaustive study of the field dependence has been attempted. In Fig. 5, we observe that the cross-conductivity L_{yx} is zero at both $\alpha = 0$ and $\alpha = \pi/6$, as expected by symmetry, and rises to a simple maximum mid-way between these endpoints. The magnitude of L_{yx} is approximately one twenty-fifth the magnitude of L_{xx}, which is consistent with a purely nonlinear effect. As only $\alpha = 0$ and $\alpha = \pi/6$ have been considered previously, this is the first time that this cross-conductivity has been calculated.

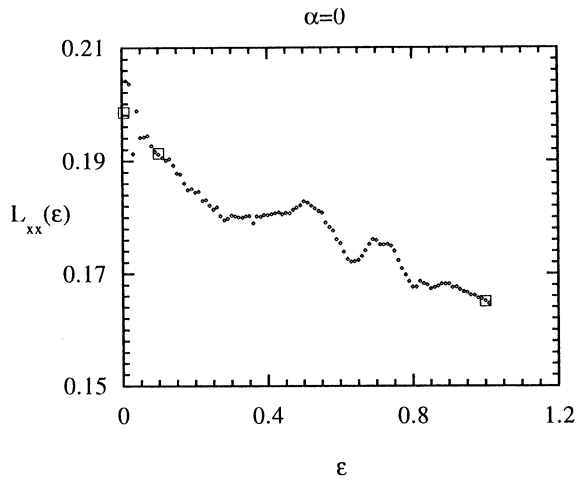

Fig. 2. Conductivity L_{xx} as a function of field at $\alpha = 0$. Each small diamond is a direct time average over 5×10^7 collisions so the error bars are less than the size of the symbols. Each square is the time average over a much longer run (10^9–10^{10} collisions), which shows the good convergence of our results.

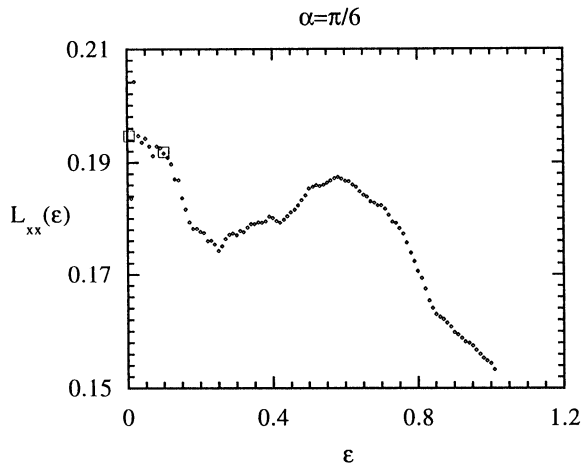

Fig. 3. Conductivity L_{xx} as a function of field at $\alpha = \pi/6$. Each small diamond is a direct time average over 5×10^7 collisions. Each square is the time average over a much longer run (as in Fig. 2).

5. Periodic Orbit Expansion for the Equilibrium Lorentz Gas

To compute the averages discussed in the previous sections, within the POE framework, a useful tool is the so-called symbolic dynamics. This consists of assigning a symbol sequence to each UPO, and it is claimed that for a UPO the symbol sequence uniquely defines the orbit. The terms in the POE can be

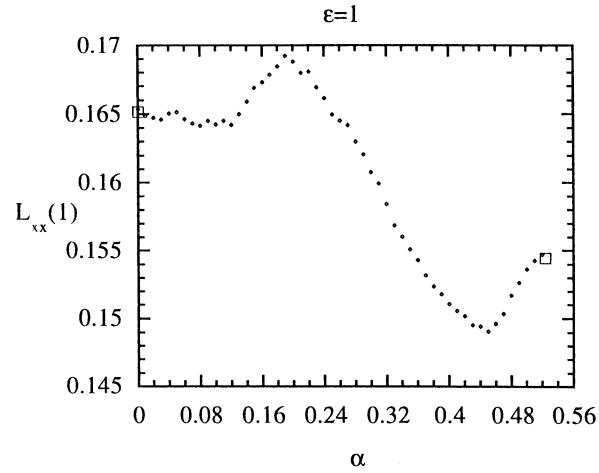

Fig. 4. Field dependent conductivity L_{xx} in the direction of the field, as a function of field angle with the field fixed at $\varepsilon = 1$. Each small diamond is a direct time average over 5×10^7 collisions. Each square is the time average over a much longer run (as in Fig. 2).

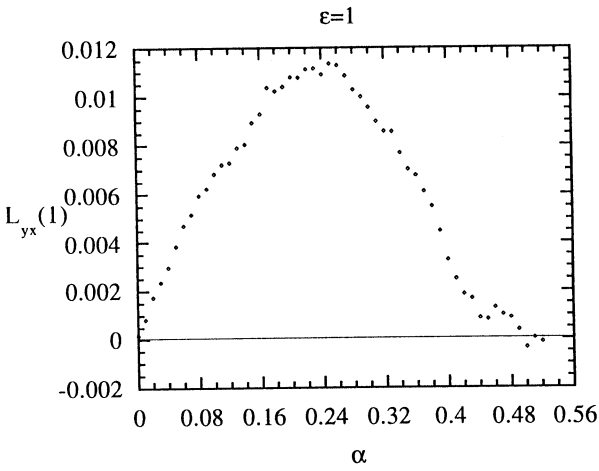

Fig. 5. Field dependent conductivity L_{yx} perpendicular to the direction of the field, as a function of field angle α with the field fixed at $\varepsilon = 1$. Each diamond is a direct time average over 5×10^7 collisions.

enumerated by determining all possible symbol sequences composed of a fixed length which are physically realisable. Sequences that contain paths that pass through scatterers must be *pruned* from that list. How many symbols are needed is an open question but for practical purposes a finite set is sufficient, especially at equilibrium. We will use symbolic dynamics to distinguish different UPOs in our simulations and to determine their degeneracy (that is the number of different orbits related by discrete symmetries).

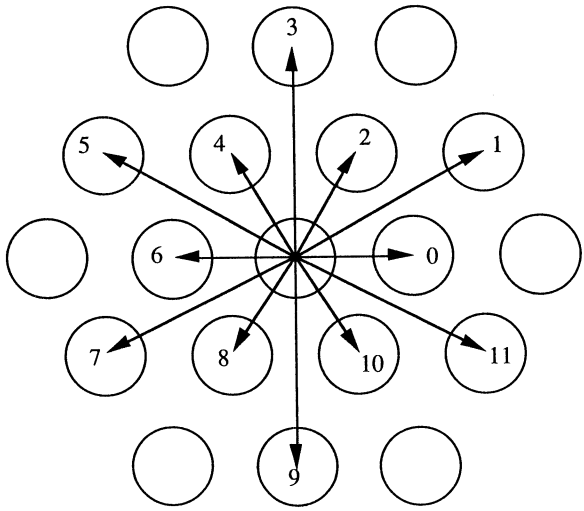

Fig. 6. Symbols associated with each of the possible flights between scatterers.

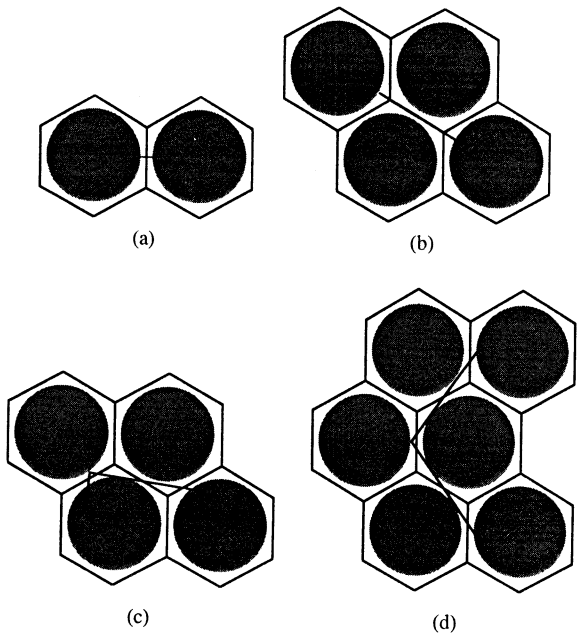

Fig. 7. Examples of length 2 UPOs: (*a*) is the (0 6) short flight orbit; (*b*) is the (5 11) long flight orbit; (*c*) is the (4 11) tick orbit; and (*d*) is the (1 5) V orbit.

To each section of trajectory between collisions we assign a symbol depending upon the vector separation of the the initial and final scatterers for that segment. In Fig. 6 we show the labels for the twelve possible flights. Due to the finite horizon, these are the only flights that are possible in the absence of a field.

At $w = 0{\cdot}2360685$ there are four types of length 2 UPOs; the short flight (S) between nearest neighbour scatterers; the long flight (L) between second nearest neighbours; the tick shaped orbit (T), consisting of a long flight and a short flight; and the V shaped orbit (V) of two long flights (see Fig. 7). It is easy to see that the S UPO can have the following symbol sequences: (0 6), (2 8), (4 10). For the long flight orbit L the possible sequences are (1 7), (3 9), (5 11). The tick shaped UPO consists of a short flight followed by a long flight and in this case there are 12 distinct symbol sequences: (0 5), (2 7), (4 9), (6 11), (8 1), (10 3), (0 7), (2 9), (4 11), (6 1), (8 3), (10 5). The last orbit V has two long flights and there are six possibilities: (7 11), (9 1), (11 3), (1 5), (3 7), (5 9). All of these six possibilities are distinct.

The total number of length 2 orbits is 24, which is made up of three S, twelve T, three L, and six V orbits. One way of thinking about these orbits is in terms of short and long flights. Short flights are between nearest neighbours and long flights are between second nearest neighbours. Clearly, it is possible for UPOs composed of two similar flights to have more symmetry than UPOs composed of different flights. This symmetry determines the degeneracy of the orbit. For the T orbit we have seen that there are 12 different symbol strings which all have the same contribution to an average property.

Table 3 presents orbits with two collisions (length 2) at $w = 0{\cdot}2360685$, giving both the fundamental symbol sequence and the degeneracy. The Lyapunov numbers are given by $\exp[\lambda\tau]$, where λ is the Lyapunov exponent, τ the period. We note that all the orbits from the groups S, L, T and V are periodic in the EC. But the S and L orbits actually are periodic in the whole phase space so that $\Delta r(t)^2$ is bounded for all t, while the T and V orbits are not closed and $\Delta r(t)^2 \sim t^2$ at large t.

Table 3. Periodic orbits of length 2

Orbit	Degeneracy	$\lambda\tau$	Symbol
S	3	1·34836495	(0 6)
T	12	3·10378194	(0 5)
L	3	3·43337893	(1 7)
V	6	4·63460493	(1 5)

All length 3 UPOs can be considered as variations upon length 2 UPOs (see Fig. 8). The first is the small triangle T made up of three short flights (which we can think of as adding an extra short flight to S). The symbol sequences for this orbit are (2 6 10), (2 10 6), (0 4 8), (0 8 4). The variation of the long flight UPO L changes one long flight into a glancing collision and hence two short flights. For example (1 7) becomes (0 2 7). The variation on the tick orbit T replaces the long flight with a glancing collision of two short flights, so that (0 5), becomes (0 4 6), which in turn becomes (0 2 6) under time reversal and rotation. This orbit consists of three short flights but is not closed. The variation on the V orbit replaces one of the long flights with a glancing collision. For example (1 5) becomes (0 2 5). The resulting orbit is open and consists of two short and one long flight. Table 4 gives the orbits with three collisions.

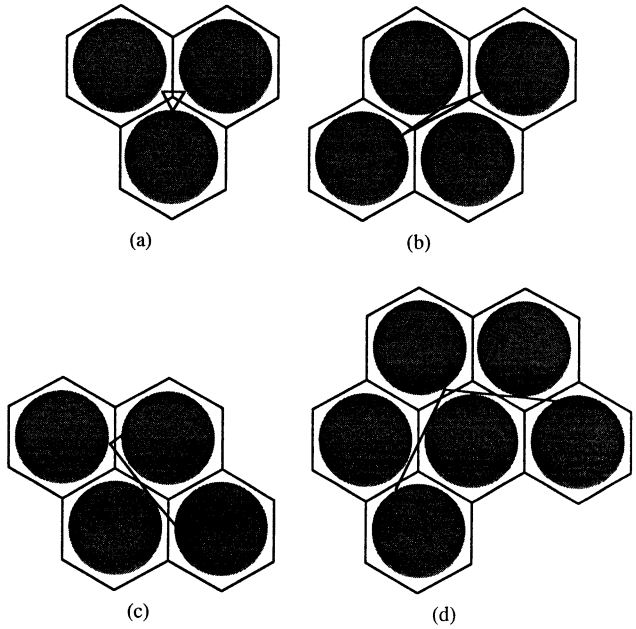

Fig. 8. Examples of length 3 UPOs. (*a*) is the (0 8 4) S′ orbit; (*b*) is the (1 6 8) L′ orbit; (*c*) is the (6 4 0) T′ orbit; and (*d*) is the (2 4 11) V′ orbit.

Table 4. Periodic orbits of length 3

Orbit	Degeneracy	$\lambda\tau$	Symbol
S′	4	3·09704399	(0 4 8)
L′	12	6·29878521	(0 2 7)
T′	24	6·84276485	(0 2 6)
V′	24	9·51433277	(0 2 5)

To explore the utility of the periodic orbit expansions, we calculate three different properties; the potential contribution to the hydrostatic pressure, the diffusion coefficient, and the average Lyapunov exponent. The average Lyapunov exponent is given by

$$\langle\lambda\rangle = \lim_{n\to\infty} \sum_{i\in P_n} \lambda_i \tau_i \Lambda_i^{-1} \Big/ \sum_{i\in P_n} \tau_i \Lambda_i^{-1} . \tag{23}$$

The potential part of the pressure p^ϕ for the system is given by

$$\langle p^\phi V\rangle = \lim_{n\to\infty} \sum_{i\in P_n} \sum_{\text{collisions}} \boldsymbol{p}.\boldsymbol{r}\Lambda_i^{-1} \Big/ \sum_{i\in P_n} \tau_i \Lambda_i^{-1} , \tag{24}$$

where $\boldsymbol{p}$ is the momentum immediately after a collision and $\boldsymbol{r}$ is the vector joining the centre of the scatterer to the point of collision.

We use a numerical scheme to search for UPOs. From a long chaotic trajectory we scan the collision sequence, at the collision time, for approximate recurrences of a phase point (θ_i, ϕ_i). If $||(\theta_{i+j}, \phi_{i+j}) - (\theta_i, \phi_i)|| < \delta$ for sufficiently small δ, then we save (θ_i, ϕ_i) as a possible initial condition for an UPO of length j. Each initial condition is then refined using a Newton–Raphson iteration scheme, and both of its Lyapunov numbers Λ_i are calculated using the method outlined in Section 7. The existence of a particular UPO ensures the existence of its time reverse, and the Lyapunov exponents for the time reverse are the negatives of those for the forward time UPO. Sampling the forward and reverse UPO as a pair ensures good convergence of the conductivity. In practice our method of sampling UPOs ensures that we sample the most probable ones thoroughly, but it is possible that UPOs with relatively high Lyapunov numbers (and hence low weight) may be neglected. The POE results for $w = 0{\cdot}2360685$ are given in Table 5.

Table 5. Periodic orbit expansion for $w = 0{\cdot}2360685$

n	# cycles	D	D^{Shanks}	$p^{\phi}V$	λ
2	24	0·3769		0·5430	1·4053
3	64	0·0901	0·2160	0·6457	2·0757
4	108	0·3146	0·2124	0·5411	1·6618
5	252	0·1269	0·2004	0·6326	1·9803
6	716	0·2477	0·2032	0·6164	1·7699
7	2184	0·1771	0·2048	0·6332	1·9733
8	5952	0·2228	0·2032	0·6511	1·8926
9	19196	0·1885	0·2011	0·6482	1·9607
10	51072	0·2084		0·6628	1·9329
direct		0·1970(10)		0·665(1)	

The results for the pressure as a function of spacing are presented in Fig. 9. At equilibrium, the pressure tensor is diagonal and the kinetic part is trivially related to the total kinetic energy.

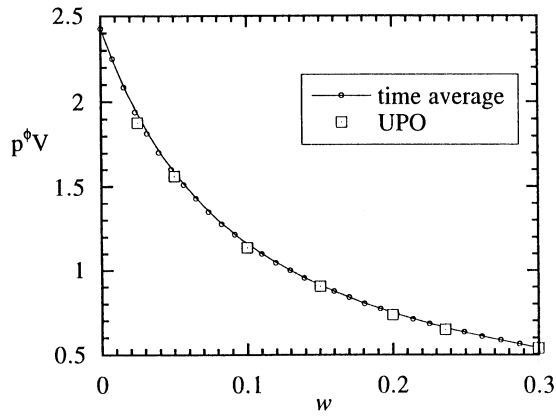

Fig. 9. Potential pressure times volume versus inter-disk spacing w. The small squares, fitted with the curve, represent the results of direct simulations of around 10^6 collisions. The large squares represent the results obtained from the use of UPO measures, as computed for UPOs up to length 12.

The fact that the POE formalism gives correct averages from the Lorentz gas suggests that there is a deeper link between the POE formalism and equilibrium statistical mechanics. In the next section we exploit this idea further.

6. Dynamical Partition Function for the Lorentz Gas

The complete framework of classical statistical mechanics can be based on two postulates (Tolman 1938; Thompson 1972). The first postulate is that of equal *a priori* probabilities for the distribution of ensemble members on the surface of constant energy, where each ensemble member is an isolated system with the same number of particles N, volume V, and energy E. This postulate implies that the **micro-canonical ensemble** has a distribution given by

$$\mathrm{d}\mu_{mc}(\Gamma) = \frac{\delta(H-E)\,\mathrm{d}\Gamma}{\int \delta(H-E)\,\mathrm{d}\Gamma} = \frac{\delta(H-E)\,\mathrm{d}\Gamma}{S(E)}\,, \tag{25}$$

where $S(E)$ is the area of energy surface $H(\Gamma) \equiv H(\boldsymbol{q},\boldsymbol{p}) = E$. This is the probability that the system will be found inside a phase space volume element $\mathrm{d}\Gamma$, centred around $\Gamma \equiv (\boldsymbol{q},\boldsymbol{p})$. It is much more usual to find that a system is not isolated, and the generic situation is to consider an equilibrium system in contact with a reservoir. An ensemble of such systems, each in contact with the same reservoir, constitutes the **canonical ensemble**. The form of the phase space distribution function for a canonical ensemble of systems can be a second postulate

$$\mathrm{d}\mu_c(\Gamma) = \frac{\mathrm{e}^{-H(\Gamma)/kT}\,\mathrm{d}\Gamma}{\int \mathrm{e}^{-H(\Gamma)/kT}\,\mathrm{d}\Gamma}\,. \tag{26}$$

Equation (26) defines what we will refer to as the canonical measure where k is Boltzmann's constant. The denominator is the canonical partition function $Z_c(N,V,T)$ which normalises the measure on the whole phase space, thus $\mathrm{d}\mu_c$ is the probability associated with the volume element $\mathrm{d}\Gamma$. The logarithm of the partition function generates the thermodynamic properties of the system, and in particular the pressure is given by the following relation:

$$p = kT\,\frac{\partial}{\partial V}\ln Z_c(N,V,T)\,. \tag{27}$$

Here we introduce a dynamical partition function for the Lorentz gas (Morriss *et al.* 1995), and what will emerge is a new dynamical basis for the microcanonical ensemble. We argue that the normalisation factor for the UPO average (equation 14) is equivalent to the canonical partition function. We define the **dynamical partition function** by

$$Z_d(V) = \lim_{n\to\infty} Z^{(n)}(V) = \lim_{n\to\infty} \sum_{i\in P_n} \tau_i \exp(-\tau_i\,\lambda_i)\,. \tag{28}$$

We have already demonstrated that the UPO measure and the microcanonical ensemble give the same averages for the Lorentz gas. If this were true for an arbitrary phase variable, then we may choose the phase variable which is equal to unity on phase element $\mathrm{d}\Gamma$ and zero elsewhere. The UPO average of this

variable would then be equal to the microcanonical probability of phase element $d\Gamma$, and we would have for the first time a dynamical basis for the assumption of equal *a priori* probability.

We observe that the dynamical partition function has the dimensions of time. This is analogous to the classical partition function for an N particle system which has the units of action to the Nth power. Before we take the logarithm we must make $Z_d(V)$ dimensionless by dividing by a characteristic time t_c, which does not affect the physics of the model. In fact it disappears in the difference between logarithms, and when partial derivatives are taken.

We now construct a numerical test for the dynamical partition function to see if it does generate the thermodynamics of the system. Integrating (27) with respect to the volume, at constant N and T we can calculate the change in the partition function for a given change in volume V, that is

$$\ln Z(V_1) - \ln Z(V_0) = \int_{V_0}^{V_1} dV \, \frac{p}{kT} = (N-1)\ln\left(\frac{V_1}{V_0}\right) + \int_{V_0}^{V_1} dV \, \frac{p^\phi}{kT}. \quad (29)$$

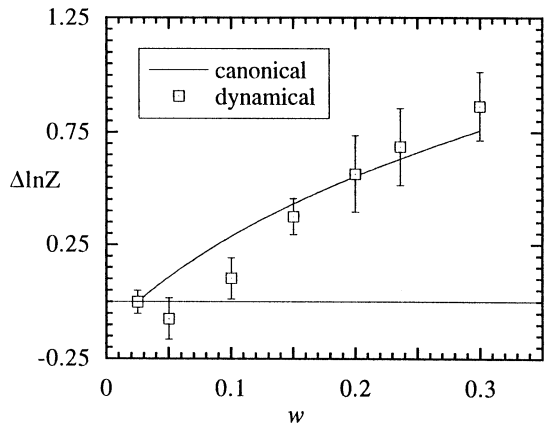

Fig. 10. Changes in the partition function. The curve represents the change of the canonical partition function obtained by integrating the pressure. The squares represent the change in the dynamical (POE) partition function.

We then evaluate $Z_d(V)$ numerically at seven different volumes. The accuracy of our estimates of $Z_d(V)$ vary. At small spacings there are significant contributions to the POEs from long orbits, whereas at higher spacings convergence is achieved at smaller lengths, but here there are sampling problems due to the much larger number of cycles. To compare with the standard thermodynamic method of equation (29) we present the change in the logarithm of the partition function as a function of spacing in Fig. 10. We choose $w_0 = 0{\cdot}025$ as our reference point, defining $\Delta \ln Z(w_0) = 0$. The results obtained by integrating the p^ϕ (referred to as canonical in Fig. 10) are highly accurate due to the accuracy of the pressure. It is observed that the proposed dynamical partition function gives results that oscillate about the canonical partition function. Because of the consistency of the slopes of the canonical and dynamical partition function results, we conclude that the dynamical partition function looks a likely candidate for a generating function

of the thermodynamics of the Lorentz gas. We note that the numerical difficulties in both calculating and enumerating all UPOs up to length 12, as we did, are formidable and probably near the limit of our present generation of computers.

7. Analytic Expressions for the Lyapunov Numbers

The Lorentz gas can be considered as a mapping rather than a continuous flow, by choosing the surface of the scatterers as the Poincaré surface of section, and studying the evolution from collision to collision. Using periodic boundary conditions, it is possible to reduce the dynamics to the surface of the scatterer in the EC. Then a point on the Poincaré surface is uniquely defined by specifying two angles (θ, ϕ) (where θ is the angle of the momentum immediately after collision, and ϕ is the position on the surface of the scatterer). The collision to collision dynamics can be represented by a mapping where

$$(\theta_{n+1}, \phi_{n+1}) = M(\theta_n, \phi_n)\,, \tag{30}$$

and where M is defined implicitly by the integrated equations of motion. Here M contains all the information required to compute the stability and thermodynamic properties of the system.

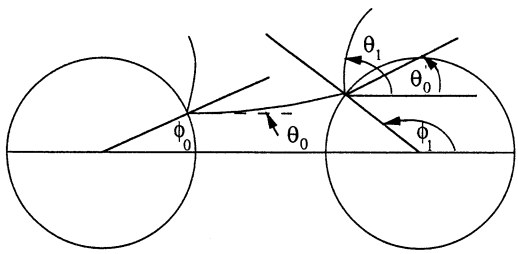

Fig. 11. Angle definitions for the free flight between collision 0 and collision 1.

The Lyapunov numbers of the periodic orbits of M can be computed as follows (Lloyd *et al.* 1995). The free flight from collision 0 to collision 1 takes (θ_0, ϕ_0) to (θ_0', ϕ_1), where θ_0 is the momentum angle immediately after collision 0, and θ_0' is the momentum angle immediately before collision 1 (see Fig. 11). This is followed by collision 1, which transforms (θ_0', ϕ_1) into (θ_1, ϕ_1). Thus, the stability matrix for one iteration of M, that is J_M, is composed of the product of the stability matrix for the free flight, J_F say, and the stability matrix for the collision, J_C. The stability matrix for a periodic orbit of n collisions is then constructed from the product of pairs of these matrices,

$$J_{\text{orbit}} = \prod_{i=1}^{n} J_M(i) = \prod_{i=1}^{n} J_C(i)\, J_F(i)\,, \tag{31}$$

where i labels the free flight, and the order of terms in the product is such that the latest collision is the left-most term. The stability matrix for the collision J_C can easily be obtained from the collision dynamics. Consider a collision in which (θ_0', ϕ_1) goes to (θ_1, ϕ_1). There is no change in ϕ_1, and $\theta_1 = -\theta_0' \mp \pi + 2\phi_1$, so that J_C is given by

$$J_C(1) = \begin{pmatrix} \frac{\partial\theta_1}{\partial\theta_0} & \frac{\partial\theta_1}{\partial\phi_1} \\ \frac{\partial\phi_1}{\partial\theta_0'} & \frac{\partial\phi_1}{\partial\phi_1} \end{pmatrix} = \begin{pmatrix} -1 & 2 \\ 0 & 1 \end{pmatrix} \tag{32}$$

which is independent of the collision geometry, so we drop the index i.

Although it is not possible to give a closed form for the part of the mapping M which corresponds to a free flight, we can calculate partial derivatives implicitly from the equations of motion given the values of $(\theta_{n+1}, \phi_{n+1})$. So the stability matrix for the free flight connecting (θ_0, ϕ_0) to (θ_0', ϕ_1) can be shown to be

$$J_F(1) = \begin{pmatrix} \frac{\sin\theta_0'}{\sin\theta_0}\frac{\cos(\phi_1-\theta_0)}{\cos(\phi_1-\theta_0')} & -\varepsilon\sin\theta_0'\frac{\sin(\phi_1-\phi_0)}{\cos(\phi_1-\theta_0')} \\ \frac{1}{\varepsilon\sin\theta_0}\frac{\sin(\theta_0'-\theta_0)}{\cos(\phi_1-\theta_0')} & \frac{\cos(\phi_0-\theta_0')}{\cos(\phi_1-\theta_0')} \end{pmatrix}. \tag{33}$$

The eigenvalues of $(J_{\text{orbit}}\, J^*_{\text{orbit}})^{\frac{1}{2}}$ (where the asterisk denotes the adjoint) are the Lyapunov numbers (Eckmann and Ruelle 1985) for a periodic orbit, which we denote by Λ_1 and Λ_2. These are related to the Lyapunov exponents λ_i by $\Lambda_i = \exp(\lambda_i\ \tau_i)$, where τ_i is the period of the orbit.

A very useful result follows from consideration of the determinant of the stability matrix. Note that $\det(J_C) = -1$ and using the collision dynamics it can be shown that

$$\det(J_F(1)) = -\frac{\sin\theta_0'}{\sin\theta_0}\frac{\cos(\phi_0-\theta_0)}{\cos(\phi_1-\theta_1)}.$$

It follows that the determinant of the stability matrix for a full **periodic** orbit is

$$\det(J_{\text{orbit}}) = \prod_{i=1}^{n}\det(J_F(i))\det(J_C) = \prod_{i=1}^{n}\frac{\sin\theta_{i-1}'}{\sin\theta_{i-1}}. \tag{34}$$

It is well known that a relation holds between the average current and average Lyapunov exponents for a system of particles, that is

$$\langle v_x\rangle = \frac{\langle\Delta x\rangle}{\tau} = \frac{\langle\lambda_1\rangle + \langle\lambda_2\rangle}{\varepsilon}. \tag{35}$$

However, the fact that equation (35) is an identity for individual UPOs can be proved using the properties of the stability matrices we have constructed. First, we note that the displacement for the ith free flight is

$$\Delta x_i = x_i - x_{i-1} = \frac{1}{\varepsilon}\ln\left(\frac{\sin\theta_{i-1}'}{\sin\theta_{i-1}}\right), \tag{36}$$

so the total displacement in the x direction during a complete cycle Δx can be written as

$$\Delta x = \sum_{i=1}^{n}\Delta x_i = \frac{1}{\varepsilon}\sum_{i=1}^{n}\ln\left(\frac{\sin\theta_{i-1}'}{\sin\theta_{i-1}}\right) = \frac{1}{\varepsilon}\ln\prod_{i=1}^{n}\left(\frac{\sin\theta_{i-1}'}{\sin\theta_{i-1}}\right) = \frac{1}{\varepsilon}\ln(\det|J_n|). \tag{37}$$

Combining this with equation (36), the PO sum rule follows immediately:

$$\varepsilon \Delta x = (\lambda_1 + \lambda_2)\tau \,. \tag{38}$$

This result proves to be very useful in analysing the properties of periodic orbits, particularly the stable ones which appear at larger values of the field.

8. Periodic Orbit Expansion for the Nonequilibrium Lorentz Gas

To demonstrate the convergence of the POE for nonequilibrium steady states, we calculate the potential contribution to the hydrostatic pressure, the conductivity, and the average Lyapunov exponent. For the Lorentz gas in an external field, we take the diffusion coefficient to be given by

$$\begin{aligned} L_{xx}(\varepsilon) = \frac{J_x(\varepsilon)}{\varepsilon} &= \lim_{n\to\infty} \frac{1}{\varepsilon} \sum_{i\in P_n} \int_0^{\tau_i} p_x(s)\, \mathrm{d}s\, \Lambda_i^{-1} \Big/ \sum_{i\in P_n} \tau_i \Lambda_i^{-1} \\ &= \lim_{n\to\infty} \frac{1}{\varepsilon} \sum_{i\in P_n} \Delta x_i \Lambda_i^{-1} \Big/ \sum_{i\in P_n} \tau_i \Lambda_i^{-1} \,. \end{aligned} \tag{39}$$

The first equality defines a field dependent conductivity. As $\varepsilon \to 0$, we can distinguish two classes of UPOs: a class of orbits with $\Delta x_i = 0$, which can be ignored, and a class for which $\Delta x_i \neq 0$. Each orbit with $\Delta x_i \neq 0$ has its time reverse, with exactly opposite displacement, $\Delta x_{-i} = -\Delta x_i$. The contribution to the numerator of equation (39) of each such pair of orbits is

$$\begin{aligned} \Delta x_i \big(\Lambda_i^{-1} - \Lambda_{-i}^{-1}\big) &= \Delta x_i \big(\mathrm{e}^{-\lambda_i \tau_i} - \mathrm{e}^{\lambda_{-i}\tau_i}\big) = \Delta x_i\, \mathrm{e}^{-\lambda_i\tau_i} \big(1 - \mathrm{e}^{(\lambda_i+\lambda_{-i})\tau_i}\big) \\ &= \Delta x\, \mathrm{e}^{-\lambda_i\tau_i} \big(1 - \mathrm{e}^{\varepsilon \Delta x_i}\big) = -\varepsilon \Delta x_i^2\, \Lambda_i^{-1} + \mathrm{O}(\varepsilon^2) \,, \end{aligned} \tag{40}$$

where the second last equality is a consequence of the PO sum rule, and we use the fact that the largest Lyapunov exponent of an orbit equals the negative of the smallest Lyapunov exponent of its time reverse. When $\varepsilon \to 0$, we have $\Lambda_i^{-1} \to \Lambda_{i0}^{-1}$, where Λ_{i0}^{-1} is the inverse Lyapunov number at zero field. Thus, combining equations (40) and (39), we recover the UPO based mean square displacement formula for the diffusion coefficient at zero field.

To demonstrate the POE method we consider the results at a spacing of $w = 0{\cdot}2360685$, at a field of $\varepsilon = 0{\cdot}1$. We observe that the contribution to the conductivity L_{xx} oscillates with the length n of the UPOs, and then the Shanks transformation gives a better estimate of the converged result (see Table 6).

In Fig. 12 we show the improved convergence of the conductivity obtained using the Shanks transformation. In Table 7 we compare the best estimates obtained for the pressure, Lyapunov exponent and conductivity using the POE method with those obtained by direct simulation.

9. The Bifurcation Diagram

Here we study the behaviour of the map M defined at the beginning of Section 4, as a function of the applied external field and we restrict our considerations to the case where $\alpha = 0$. In order to visualise the behaviour of M we consider the projection of the mapping onto the θ-axis. We find a quite complex structure, which resembles the bifurcation diagram of a one-dimensional dynamical system (Lloyd *et al.* 1994).

Table 6. Periodic orbit expansion and Shanks transformation at $\epsilon = 0{\cdot}1$ and $\alpha = 0$

n	# cycles	L_{xx}	L_{xx}^{Shanks}	$p^{\phi}V$	λ
2	9	0·4766		0·8470	1·5688
3	30	0·0859	0·2147	0·7867	2·0150
4	73	0·2780	0·2044	0·7987	1·6635
5	198	0·1586	0·1917	0·7123	2·0822
6	550	0·2043	0·1862	0·7114	1·8687
7	1710	0·1742	0·1857	0·6633	1·9801
8	4817	0·1928	0·1893	0·6646	1·9297
9	13460	0·1885	0·1906	0·6306	1·9697
10	33966	0·1926		0·6277	1·9477

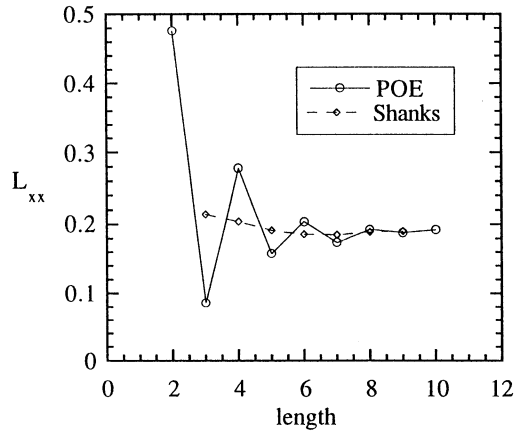

Fig. 12. Periodic orbit expansion and Shanks transformation results at $\varepsilon = 0{\cdot}1$ and $\alpha = 0$, showing the convergence of the conductivity.

Table 7. POE average properties

The second and third columns contain the direct simulation results for the diffusion coefficient and the pressure. The POE estimates are based on the Shanks transformation for the conductivity and the best available result for the pressure and average Lyapunov exponent. Notice that the values of the pressure obtained from POE are within 3% of the direct simulation results, and those for the diffusion coefficient are within 1% or better. Here α is the angle between the (0 6) short flight and the field direction

α	ε	L_{xx}	$p^{\phi}V$	$\langle L_{xx}\rangle_{\text{UPO}}$	$\langle p^{\phi}V\rangle_{\text{POE}}$	$\langle\lambda\rangle_{\text{POE}}$
0	0·0	0·197(1)	0·665(1)	0·201(3)	0·69(5)	1·94(2)
0	0·005	0·2006(1)	0·6608(1)	0·200(6)	0·66(3)	1·95(1)
0	0·1	0·1918(1)	0·6606(1)	0·191(2)	0·63(3)	1·96(1)
0	1·0	0·165(1)	0·6866(1)	0·168(8)	0·65(5)	1·71(5)
$\pi/6$	0·0	0·197(1)	0·665(1)	0·201(3)	0·69(5)	1·94(2)
$\pi/6$	0·005	0·195(1)	0·6608(1)	0·196(5)	0·66(3)	1·96(1)
$\pi/6$	0·1	0·192(1)	0·6606(1)	0·185(8)	0·66(3)	1·97(1)

In Fig. 13 we present the upper half of the θ–ε diagram, obtained by direct iteration of a few initial conditions, ignoring the initial transient behaviour. The other half of this diagram is trivially obtained from this by reflection in the line $\theta = 0$. When the field is varied, a series of dramatic changes in the dynamics of

the mapping occur. For fields of $2{\cdot}1$ or less the iterations of the initial conditions sample most of the θ-space. For $2{\cdot}1 < \varepsilon < 2{\cdot}629$, a wide variety of dynamics emerges. For $\varepsilon > 2{\cdot}629$, the iterations settle onto a stable length 2 orbit with symbol string (4 8), shown in Fig. 14. Note that the curvature of a free flight grows with increasing field. Eventually, as the external field grows to infinity, the unique stable orbit which survives approaches an orbit composed of horizontal straight lines, and arcs of circumference. As a consequence, in the limit $\varepsilon \to \infty$, the diffusion coefficient goes to zero. For all fields larger than $2{\cdot}629$, there is a unique stable orbit, and its basin of attraction is the whole phase space, except for the points which lie in the unstable (0 6) length 2 orbit.

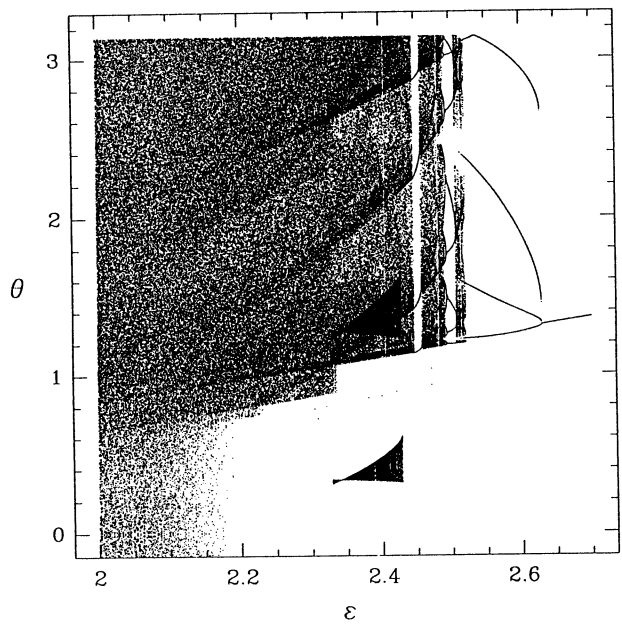

Fig. 13. Upper half of the bifurcation diagram for the discrete mapping $M(\phi, \theta)$ as a function of field ε, projected onto the (ε, θ) plane. This diagram is symmetrised by mapping $(-\theta) \Rightarrow \theta$. Above $\varepsilon \approx 2{\cdot}62902$ there is a single line which is the stable (4 8) length 2 orbit, which then becomes a stable length 8 orbit. After that, there are chaotic bands interspersed with periodic windows. The separate feature at $2{\cdot}3 < \varepsilon < 2{\cdot}46$ is one example of the neutrally stable elliptical orbit $(4\,10)^{\infty}$.

As a dynamical system, the range of fields $2{\cdot}1 < \varepsilon < 2{\cdot}629$ is of particular interest. To understand what happens here, we follow the fate of the stable (4 8) orbit, as ε is lowered through $2{\cdot}629$. We see that the curvature of the free flights in the stable (4 8) orbit decreases, until they both develop zero-effect glancing collisions with another scatterer at $\varepsilon_g \approx 2{\cdot}62902433$. Any further decrease in the field *prunes* the orbit. The (4 8) orbit disappears while it is still stable, and is replaced by a length 8 orbit. We might have expected an extra collision to be introduced into each of the free flights of the length 2 orbit, thus producing a length 4 orbit. However, each additional collision introduces more instability to

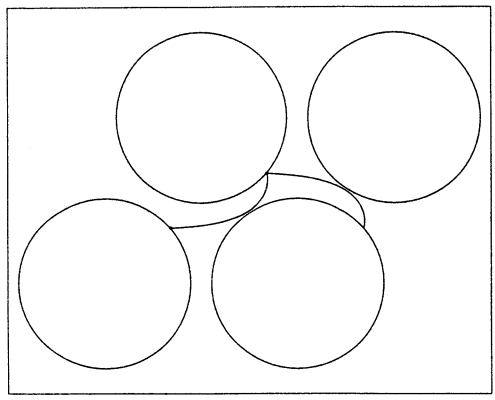

Fig. 14. Stable length 2 orbit (48) at $\varepsilon = 2{\cdot}7$. As the field is in the negative x-direction, the wandering particle moves from right to left.

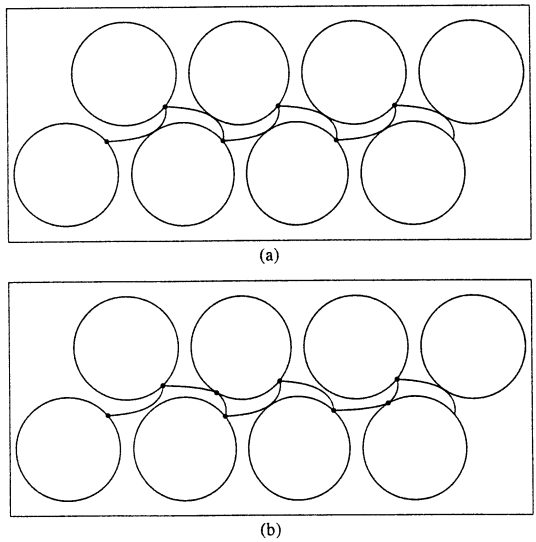

Fig. 15. (a) Three copies of the stable length 2 orbit (48) just before it is pruned at $\varepsilon \approx 2{\cdot}629$. If the field is decreased further, the curved part intersects the scatterer. (b) The same as (a) except that the field has been reduced further to $\varepsilon = 2{\cdot}625$, and the stable length 2 orbit has been pruned. It is replaced by a stable length 8 orbit (26841064 8) which is similar to the three copies of (48) but has two extra collisions.

the orbit. Thus, the introduction of as few as possible new collisions per free-flight ensures that the new orbit is the most stable possible. In particular, the orbit which replaces the (48) orbit, introduces only one new collision for every three free-flights. This new stable orbit has length 8, and it consists of three sequential copies of the original length 2 orbit, where only two new collisions have been added, see Fig. 15a. The length 8 orbit becomes unstable at $\varepsilon \approx 2{\cdot}50609$, and is pruned at $\varepsilon \approx 2{\cdot}5057$ (see Fig. 15b).

In the bifurcation diagram (Fig. 13), the transition (length-2)→(length-8) is expressed by the fact that, as the field is lowered, each of the original two points of the stable (4 8) orbit splits into three different points, while two new points are generated. The transformation is pruning driven, not stability driven. Clearly, although the bifurcation diagram in Fig. 13 seems reminiscent of those for one-dimensional maps, the mechanism at work is quite different.

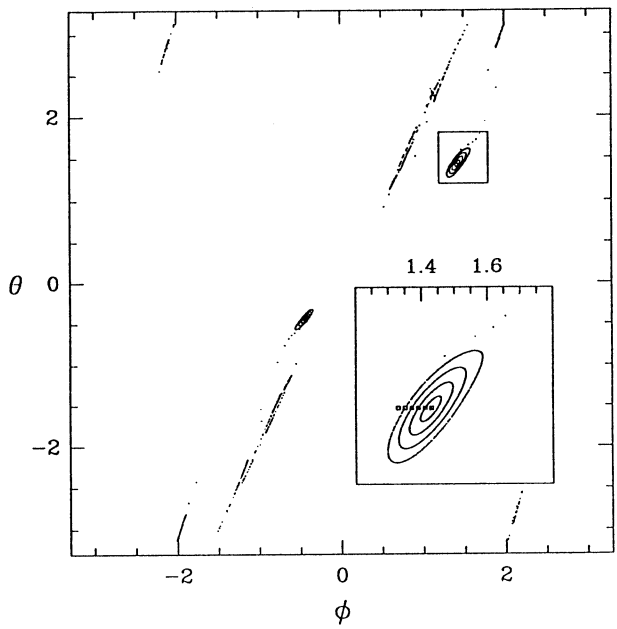

Fig. 16. Plot of the full (ϕ, θ) plane at $\varepsilon = 2 \cdot 43$ for a series of initial conditions near the neutrally stable (4 10) orbit. Around this point there is a continuum of initial conditions, each of which produces a distinct neutrally stable elliptical orbit $(4\,10)^{\infty}$, centred about the neutrally stable (4 10) orbit. In the inset, the small squares represent the initial conditions, while the other points represent their time evolution. Five of the initial conditions give elliptical orbits while the other one, after an initial transient, gives a chaotic orbit.

At still smaller fields, the simplest orbits to consider are the short-flight orbits of length 2. Among these, the (0 6) orbit is unstable at all values of the field. The (4 10) orbit however, does change in shape and stability, with field. It exists for fields in the range $0 \leq \varepsilon < 2 \cdot 46$, becoming neutrally stable at $\varepsilon \approx 2 \cdot 46$. For fields in the range $2 \cdot 3 < \varepsilon < 2 \cdot 46$ there are two different (4 10) orbits, one of which is unstable while the other is neutrally stable. However, around this second neutrally stable orbit there is a continuum of initial conditions each of which begins a distinct orbit in phase space, whose collision points fill up an ellipse in the (ϕ, θ) plane (see Fig. 16). All of these orbits have symbol string $(4\,10)^{\infty}$, where the superscript stresses that either the number of repeats is very large (for a large periodic orbit), or that the symbol sequence is repeated indefinitely without closing (a non-periodic orbit). In either case the orbit returns arbitrarily

close to the initial condition, hence the x-displacement is zero, and these orbits are non-dissipative. The presence of elliptic rather than hyperbolic trajectories shows that the hyperbolicity properties of the Lorentz gas can be lost, at some values of ε. This leads to a loss of ergodicity as time averages along elliptic orbits differ from those computed along chaotic orbits. Thus, $\varepsilon = 2{\cdot}3$ sets an upper bound for the value of the field at which ergodicity remains.

10. Concluding Remarks

In this paper we have reviewed the formalism of POE, and its applications to systems of interest in statistical physics, such as the equilibrium and nonequilibrium Lorentz gas. In particular, we have seen that POEs reproduce the correct averages for thermodynamic, and dynamic quantities, which make them suitable to study the phase space distribution functions. This fact has been used to infer the possibility that the normalisation of the UPO measures plays the role of the partition function, at equilibrium. Our test of such a hypothesis is encouraging, although the numerical difficulties met in such an endeavour seriously impair our ability to draw definite conclusions. Our results provide us with a new dynamical basis for the universally accepted hypothesis of equal *a priori* probabilities in phase space, and shows the usefulness of a detailed knowledge of the microscopic structure of phase space. If this program can be carried over to nonequilibrium systems, we will have, for the first time, a dynamically based distribution function for nonequilibrium. Our results are encouraging also in this direction, although the numerical difficulties that are found in the study of nonequilibrium models are even harder than at equilibrium.

The last part of our work, devoted to the study of the nonequilibrium Lorentz gas as a two-dimensional mapping, shows that this statistical mechanical model has many interesting features from a purely dynamical systems point of view. Moreover, a partial answer is found to the question of what is the value of the external field for which ergodicity breaks down (Chernov *et al.* 1993), which is important to know as it sets a bound on the validity of the rigorous results recently derived for such a system.

Acknowledgments

This work has been supported by the Australian Research Council (A69131116). LR gratefully acknowledges partial support from GNFM-CNR (Italy).

References

Artuso, R., Aurell, E., and Cvitanovic, P. (1990). *Nonlinearity* **3**, 325 & 361.

Baranyai, A., Evans, D. J., and Cohen, E. G. D. (1993). *J. Stat. Phys.* **70**, 1085.

Chernov, N. I., Eyink, G. L., Lebowitz, J. L., and Sinai, Ya. G. (1993). *Phys. Rev. Lett.* **70**, 220; *Comm. Math. Phys.* **154**, 569.

Cvitanovic, P. (1992). *In* 'Applied Chaos' (Eds J. H. Kim and J. Stringer), p. 413 (Wiley: New York).

Cvitanovic, P., Gaspard, P., and Schreiber, T. (1992). *Chaos* **2**, 85.

Eckmann, J. P., and Ruelle, D. (1985). *Rev. Mod. Phys.* **57**, 617.

Evans, D. J., and Morriss, G. P. (1990). 'Statistical Mechanics of Nonequilibrium Liquids' (Academic: London).

Evans, D. J., Cohen, E. G. D., and Morriss, G. P. (1990). *Phys. Rev.* A **42**, 5990.

Gaspard, P., and Rice, S. A. (1989). *J. Chem. Phys.* **90**, 2225, 2242 & 2255.

Grebogi, C., Ott, E., and Yorke, J. A. (1988). *Phys. Rev.* A **37**, 1711.
Hannay, J. H., and Ozorio de Almeida, A. M. (1984). *J. Phys.* A **17**, 3429.
Lloyd, J. P., Niemeyer, M., Rondoni, L., and Morriss, G. P. (1995). *Chaos* **5**, 3.
Lloyd, J. P., Rondoni, L., and Morriss, G. P. (1994). *Phys. Rev.* E **50**, 3416.
Lorentz, H. A. (1905). *Proc. Amst. Acad.* **7**, 438.
Machta, J., and Zwanzig, R. (1983). *Phys. Rev. Lett.* **50**, 1959.
Moran, B., and Hoover, W. G. (1987). *J. Stat. Phys.* **48**, 709.
Morriss, G. P., and Rondoni, L. (1994). *J. Stat. Phys.* **75**, 553.
Morriss, G. P., Rondoni, L., and Cohen, E. G. D. (1995). *J. Stat. Phys.* **80**, 35.
Parry, W. (1986). *Comm. Math. Phys.* **106**, 267.
Rondoni, L., Morriss, G. P., Lloyd, J. P., Niemeyer, M., and Cohen, E. G. D. (1995). Proc. Int. Conf. on Dynamical Systems and Chaos, Vol. 12, p. 434 (World Scientific: Singapore).
Thompson, C. J. (1972). 'Mathematical Statistical Mechanics' (Macmillan: New York).
Tolman, R. C. (1938). 'The Principles of Statistical Mechanics' (Oxford University Press: London).
Vance, W. N. (1992). *Phys. Rev. Lett.* **69**, 1356.

Manuscript received 6 December 1994, accepted 1 February 1995